Chaotic Modeling and Simulation (CMSIM) 1: 61-68, 2011

Routes to chaos in confined thermal convection arising from a cylindrical heat source

Diego Angeli[1], Arturo Pagano[2],
Mauro A. Corticelli[1], and Giovanni S. Barozzi[1]

[1] University of Modena and Reggio Emilia, Department of Mechanical and Civil Engineering, Via Vignolese, 905, I-41125 Modena, Italy
(E-mail: diego.angeli@unimore.it)
[2] University of Catania, Department of Industrial and Mechanical Engineering Viale Andrea Doria, 6, I-95125 Catania, Italy
(E-mail: apagano@diim.unict.it)

Abstract. Natural convection flows arising from a horizontal cylinder centred in a square-sectioned enclosure are studied numerically. The sequence of bifurcations marking the transition of base fixed-point solutions to unsteady, chaotic flows is followed for increasing values of the Rayleigh number, and for two values of the enclosure aspect ratio, A. It is observed that, for the lower A-value, the route to chaos is triggered by a supercritical Hopf bifurcation, followed by a sequence of period-doublings, while, for the higher A-value, the symmetry of the system is broken by a pitchfork bifurcation, with periodic orbits originating from both branches, and eventually approaching chaos, exhibiting features typical of blue-sky catastrophes.
Keywords: Thermal convection, transition to chaos, bifurcations, period-doubling.

1 Introduction

Buoyancy-induced flows in enclosures are very complex in nature, and highly unpredictable, due to the bi-directional interaction between the flow and temperature fields, and the sensitivity of the thermal-flow regimes to the geometric and thermal configuration of the system.

The importance of bifurcations and chaos in buoyancy-induced flows as a research topic goes far beyond the field of thermal sciences. In fact, it is deeply entwined with the history of chaos theory, since the discovery of the renown Lorenz attractor, originating from a simplified Rayleigh-Bénard convection model [1]. From that seminal study, many works have been carried out on the non-linear dynamics of thermal convection in basic enclosure configurations, such as the rectangular enclosures heated from below and from the side [2,3], and, more recently, the horizontal annulus between two coaxial cylinders [4]. Fewer works dealt with more complex geometrical and thermal configurations [5,6]. Nevertheless, from a theoretical and practical standpoint, the interest in this topic is growing continuously.

Received: 11 July 2011 / Accepted: 28 October 2011

ISSN 2241-0503

The physical system considered in the present study is the cavity formed by an infinite square parallelepiped with a centrally placed cylindrical heating source. The system is approximated to its 2D transversal square section containing a circular heat source, as sketched in Fig. 1. The temperature of both enclosure and cylinder is assumed as uniform, the cylindrical surface being hotter than the cavity walls. The resulting flow is investigated with respect to the leading parameter of the non-dimensionalized problem, the Rayleigh number Ra, based on the gap width H, and for two values of the aspect ratio $A = L/H$, between the cavity side length and the minimum enclosure to cylinder gap width, namely $A = 2.5$ and $A = 5$. The third parameter of the system, the Prandtl number, is fixed at a value $Pr = 0.7$, representative of air at environmental conditions.

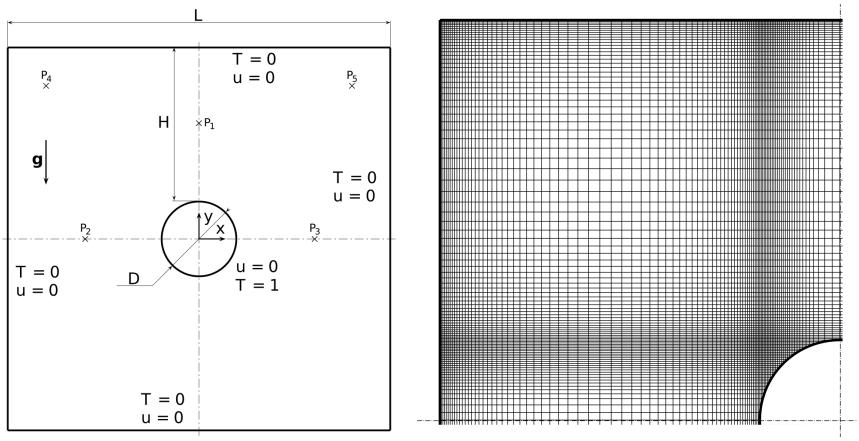

Fig. 1. Left: schematic of the system under consideration; (×) symbols indicate locations of the sampling points. Right: quadrant of the computational grid for $A = 2.5$.

Numerical predictions are carried out by means of a specifically developed finite-volume code. Successive bifurcations of the low-Ra fixed point solution are followed for increasing Ra. To this aim, time series of the dependent variables (velocity components and temperature), are extracted in 5 locations represented in Fig. 1 by points P1 to P5. Nonlinear dynamical features are described by means of phase-space representations, power spectra of the computed time series, and of Poincaré maps.

2 Numerical method

The problem is stated in terms of the incompressible Navier-Stokes formulation, under the Boussinesq approximation. The governing equations (continuity, momentum and energy) are tackled in their non-dimensional form:

$$\nabla \cdot \mathbf{u} = \mathbf{0} \tag{1}$$

$$\frac{\partial \mathbf{u}}{\partial t} + \mathbf{u} \cdot \nabla \mathbf{u} = -\nabla p + \frac{Pr^{1/2}}{Ra^{1/2}} \nabla^2 \mathbf{u} + T\hat{\mathbf{g}} \tag{2}$$

$$\frac{\partial T}{\partial t} + \mathbf{u} \cdot \nabla T = \frac{1}{(RaPr)^{1/2}} \nabla^2 T \tag{3}$$

where t, $\mathbf{u}$, p and T represent the dimensionless time, velocity vector, pressure and temperature, respectively, and $\hat{\mathbf{g}}$ is the gravity unit vector. A value $Pr = 0.7$ is assumed for air. Boundary conditions for T and $\mathbf{u}$ are reported in Figure 1.

The numerical technique adopted is based on a second-order, Finite Volume implementation of equations (1)-(3) on non-uniform Cartesian grids: a more detailed description of the spatial and temporal discretization schemes is found in [7]. The 2D modelling of arbitrarily irregular boundaries on Cartesian grids is achieved thanks to the original scheme developed by Barozzi *et al.* [8], which preserves second-order accuracy for the method, as well as the computational efficiency of the Cartesian approach.

In view of the work objectives, special care was put on the grid sizing of both near-wall areas and internal domain regions, as shown in Fig. 1. The average cell spacing in each region was chosen according to scaling considerations, as illustrated in [6]. The time step size has been chosen small enough so as to ensure a suitably accurate reproduction of the continuous-time system dynamics.

For either A-value, the initial conditions were chosen so as to follow the evolution of low-Ra base-flow, fixed-point solutions [7]. In order to detect the occurrence of successive bifurcations, Ra was increased monotonically with suitable steps, each simulation starting from the final frame of the preceeding one. All the simulations were protracted to steady-state or, when unsteady flows were detected, until a fixed dimensionless time span was covered.

$A = 2.5$ (190×190 grid)	
Ra	Bifurcation
4×10^4	S (base flow)
$6.6 \sim 6.8 \times 10^4$	$S \to P_1$ (supercritical Hopf)
$1.7 \sim 1.8 \times 10^5$	$P_1 \to P_2$ (period-doubling)
$1.8 \sim 1.9 \times 10^5$	$P_2 \to P_4$ (period-doubling)
$1.9 \sim 2.0 \times 10^5$	$P_4 \to \ldots \to N$

$A = 5$ (288×288 grid)	
Ra	Bifurcation
1.8×10^4	S (base flow)
$3.2 \sim 3.4 \times 10^4$	$S \to NS$ (pitchfork)
$6.0 \sim 7.0 \times 10^4$	$NS \to P$ (Hopf)
$6.0 \sim 7.0 \times 10^5$	$P \to N$ (Blue-sky catastrophe)

Table 1. Bifurcations of the low-Ra base flow solution for each A.

3 Results and discussion

Table 2 summarizes the sequences of bifurcations leading to chaos for both values of the aspect ratio A. The nomenclature used in defining the different types of asymptotic behaviours follows the systematic introduced by Angeli *et al.* [4]. In the following, details of both routes are briefly illustrated by means of established nonlinear analysis tools.

For $A = 2.5$, starting from the base solution at $Ra = 4 \cdot 10^4$, the system asymptotically reaches a fixed-point for $Ra \leq 6.6 \times 10^4$. As Ra is increased from $Ra = 6.6 \times 10^4$ to $Ra = 6.8 \times 10^4$, oscillatory behaviour sets in, until a periodic limit cycle is reached. In Fig. 2, 2D projections of the corresponding T-u_x-u_y attractors are plotted as a function of Ra. The passage from the lower-Ra fixed-point solution to the periodic orbit is clearly portrayed, thus suggesting the occurrence of a Supercritical Hopf bifurcation.

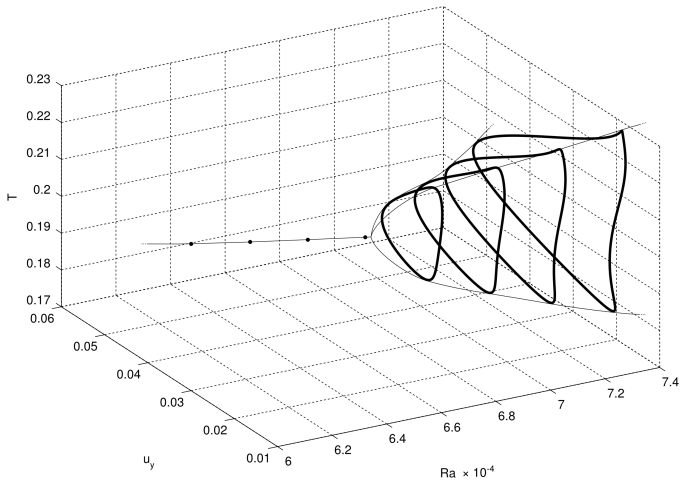

Fig. 2. Sequence of 2D attractors u_y-T at point P2, for $A = 2.5$ and for increasing Ra.

Fig. 3 reports the power spectral density distribution of the temperature time series at point P1 for the case $A = 2.5$ and for increasing values of the Rayleigh number. The values of Ra have been chosen with the aim of showing the occurrence of a period doubling route to chaos which characterises the evolution of the system dynamics for the mentioned aspect ratio. In fact, it is possible to observe that the two original fundamental harmonics observed in the power spectrum of temperature at $Ra = 1.7 \times 10^5$ become four for $Ra = 1.8 \times 10^5$ and double again for $Ra = 1.9 \times 10^5$; the last case, at $Ra = 2.0 \times 10^5$, is instead characterised by a broadband power spectrum, which represents a first hint of chaotic dynamics, with the broadened bands arising around the original harmonics of the previous cases.

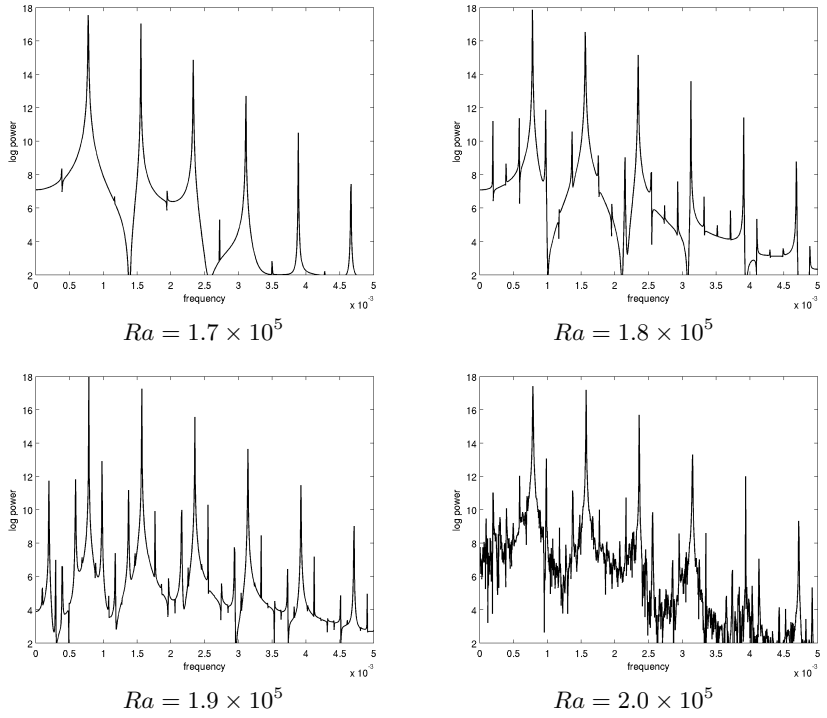

$Ra = 1.7 \times 10^5$ $Ra = 1.8 \times 10^5$

$Ra = 1.9 \times 10^5$ $Ra = 2.0 \times 10^5$

Fig. 3. Power spectral density of T at point P1, for $A = 2.5$ and for increasing Ra

This observation is confirmed by the analysis of the system attractors reported in the T-u_x-u_y state space, as reported in Fig. 4. Considering that each of the fundamental harmonics observed in the power spectrum corresponds to a loop of the attractor in the phase space representation, it is possible to observe that the original two-loop limit cycle at $Ra = 1.7 \times 10^5$ gives rise to a four-loop limit cycle at $Ra = 1.8 \times 10^5$, which, in turn, is doubled again in a eight-loop limit cycle at $Ra = 1.9 \times 10^5$. Finally, for the last of the reported values of Ra, $Ra = 2.0 \times 10^5$, in accordance with previous observations on the power spectrum, the attractor shows a chaotic morphology, with fractal bands distributed around the loops of the original limit cycles.

Fig. 4 reports also the intersections of the 3-dimensional attractors with Poincaré surfaces of section that have been obtained considering the plane u_x-T passing by the mean values of the calculated time series of the state variable u_y. Such intersections have been reported in the maps in Fig. 5. It is observed that a couple of intersections arises for each loop of the limit cycle. Again, the successive period doublings can be observed by spanning the maps at $Ra = 1.7 \times 10^5$ to $Ra = 1.8 \times 10^5$ and, then, to $Ra = 1.9 \times 10^5$, whereas ordered series of intersections, typical of deterministic chaotic dynamics, characterise the Poincaré map at $Ra = 2.0 \times 10^5$. For brevity, it is just mentioned here that an accurate observation of the local structure of such series of intersections reveals the stretching and folding typical of fractal sets.

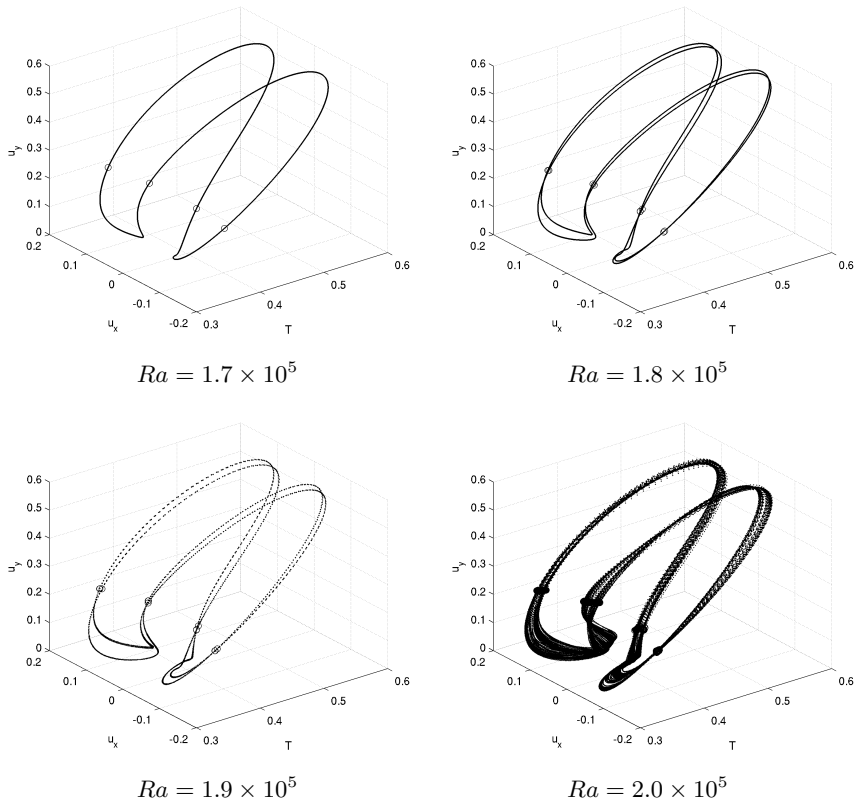

Fig. 4. 3D attractor in state space T-u_x-u_y at point P1, for $A = 2.5$ and for increasing Ra

For the higher value of the aspect ratio A considered, $A = 5$, the system undergoes a different sequence of bifurcations leading to chaos. Fig. 6(a) represents the evolution of the T-u_y attractors at point P2 as a function of Ra. As Ra is increased beyond $Ra = 3.2 \times 10^4$, the base flow becomes unstable, and gives rise to two different solution branches, suggesting the occurrence of a pitchfork bifurcation (whose sub- or supercritical nature is still to be ascertained). The two solution branches correspond to stable mirrored dual solutions [6].

By further increasing Ra, each of the two solution branches undergo a Hopf bifurcation to a periodic limit cycle, as clearly visible in Fig. 6(a). Such transition occurs between $Ra = 6 \times 10^4$ and $Ra = 7 \times 10^4$. The periodic orbits remain stable for a wide range of Ra-values, up to $Ra = 6 \times 10^5$. From Fig. 6(b), a progressive increase of the period of the limit cycle, *i.e.* of the loop extension can be appreciated. This trend eventually leads to the chaotic attractor reported in Fig. 6(c), for $Ra = 7 \times 10^5$, in a general evolution which seems to belong to the class of blue-sky catastrophes [9]. Such an observation deserves further analyses which, however, are beyond the scope of the present study.

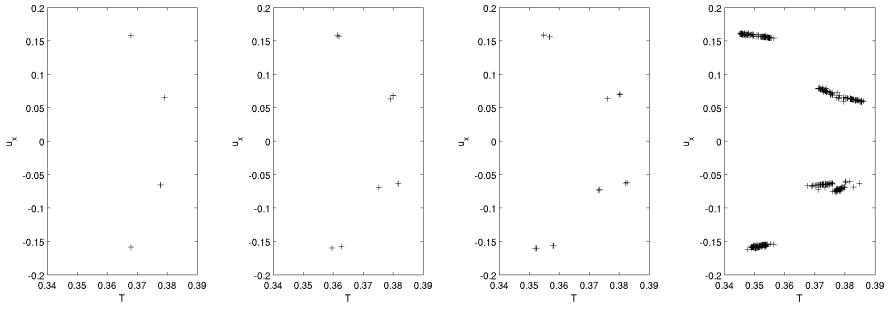

Fig. 5. Poincaré surfaces of section of the 3D attractors at point P1, for $A = 2.5$ and for increasing Ra

4 Concluding remarks

Natural convection flows arising from a horizontal cylindrical source centred in a square enclosure were investigated numerically. Two values of the aspect ratio A were considered; for which the entire scenario leading to deterministic chaos was outlined, for increasing values of the Rayleigh number.

For the lower A-value, $A = 2.5$, the flow undergoes a Hopf bifurcation, followed by a sequence of period-doublings. For the higher A-value, $A = 5$, a pitchfork bifurcation gives rise to stable periodic orbits, persisting for a large range of Ra-values. Chaotic behaviour is finally observed, on top of an evolution which resembles a blue-sky catastrophe.

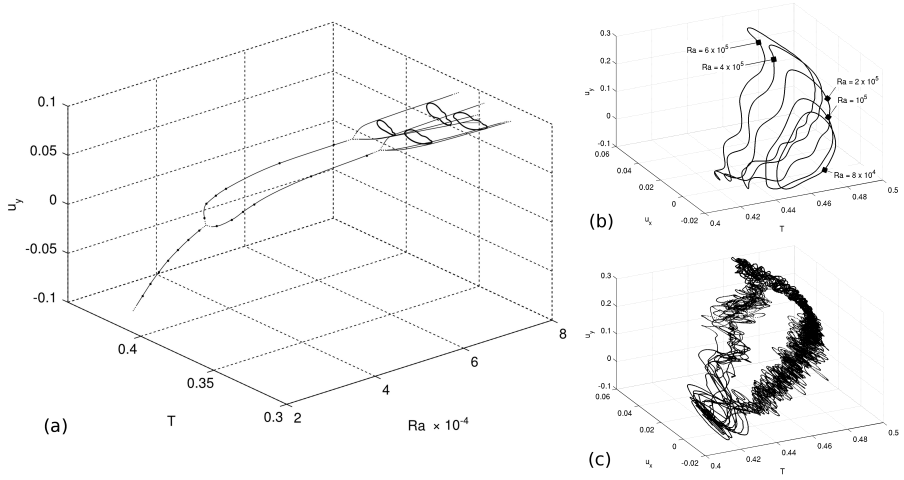

Fig. 6. (a) Sequence of 2D attractors T-u_y at point P2, for $A = 5$ and for increasing Ra; (b) 3D periodic orbits in state space T-u_x-u_y at point P1, for $A = 5$ and for increasing Ra; (c) chaotic attractor at point P1, for $A = 5$ and $Ra = 7 \times 10^5$.

References

1.E. N. Lorenz. Deterministic nonperiodic flow. *Journal of Atmospheric Sciences*, 20:130–141, 1963.
2.K. T. Yang. Transitions and bifurcations in laminar buoyant flows in confined enclosures. ASME *Journal of Heat Transfer*, 110:1191–1204, 1988.
3.P. Le Quéré. Onset of unsteadiness, routes to chaos and simulations of chaotic flows in cavities heated from the side: a review of present status. In G. F. Hewitt, editor, *Proceedings of the Tenth International Heat Transfer Conference*, volume 1, pages 281–296, Brighton, UK, 1994. Hemisphere Publishing Corporation.
4.D. Angeli, G. S. Barozzi, M. W. Collins, and O. M. Kamiyo. A critical review of buoyancy-induced flow transitions in horizontal annuli. *International Journal of Thermal Sciences*, 49:2231–2492, 2010.
5.G. Desrayaud and G. Lauriat. Unsteady confined buoyant plumes. *Journal of Fluid Mechanics*, 252:617–646, 1998.
6.D. Angeli, A. Pagano, M. A. Corticelli, A. Fichera, and G. S. Barozzi. Bifurcations of natural convection flows from an enclosed cylindrical heat source. *Frontiers in Heat and Mass Transfer*, accepted for publication, 2011.
7.D. Angeli, P. Levoni, and G. S. Barozzi. Numerical predictions for stable buoyant regimes within a square cavity containing a heated horizontal cylinder. *International Journal of Heat and Mass Transfer*, 51:553–565, 2008.
8.G. S. Barozzi, C. Bussi, and M. A. Corticelli. A fast cartesian scheme for unsteady heat diffusion on irregular domains. *Numerical Heat Transfer B*, 46:56–77, 2004.
9.Y. Kuznetsov. *Elements of Applied Bifurcation Theory*, volume 112 of *Applied Mathematical Sciences*. Springer-Verlag, New York, 2nd edition, 1998.